A Study of Near-field Aperture Geometry Effects on Very Small Aperture Lasers (VSAL)

Fang Chen*, Amit Itagi, Larissa Stebounova**, J. A. Bain, D. D. Stancil,
G. C. Walker**, T.E. Schlesinger

Data Storage Systems Center, Department of Electrical and Computer Engineering,
Carnegie Mellon University, Pittsburgh, PA, 15213, USA
**Department of Chemistry, University of Pittsburgh, Pittsburgh, PA, 15260, USA

ABSTRACT

We have investigated nano-apertures with different geometries on VSALs using far-field measurements, near-field measurements, and finite difference time domain (FDTD) simulation methods. We were able to quantitatively verify the aperture geometry dependent power throughput in all three methods. From both far-field measurements and FDTD simulation results, we conclude that for the apertures of the same area, a rectangular aperture with the long side perpendicular to the active layer has the largest throughput, while a circular aperture has the second largest, and the rectangular aperture with the long side parallel to the active layer has the least throughput among the three. We have attempted to correlate the relationship between far-field power and near-field power. Employing an apertureless near-field scanning optical microscopy (NSOM), we found that for the two rectangular apertures being studied, the near-field power throughput result was consistent to that of far-field measurement. Using VSALs as a near-field aperture testbed was also proposed and demonstrated.

Keyword: Very small aperture laser (VSAL), Nano-aperture, Aperture Geometry, Power throughput, Far-field, Near-field, Apertureless NSOM, Finite difference time domain (FDTD), Focused ion beam (FIB)

1. INTRODUCTION

Very small aperture lasers (VSAL) consist of a semiconductor laser that has a sub-wavelength aperture in the exit pupil. The light coupled out from the aperture is confined spatially and maintains a constant power in the near-field regime. Therefore, VSALs are a promising candidate for near-field optical recording or as hybrid recording light sources [1]. Because the aperture is directly fabricated on the front facet of the laser, it is also an ideal tool for investigating aperture performance in the near-field. From both experimental and theoretical data, one would expect that as the aperture size is decreased, the power that is transmitted through the aperture (throughput) would drop quickly. As a result, if a constant transmitted power density is desired, one must design apertures with high throughput efficiency for small apertures. Aperture design entails selecting the size, shape and materials used to form apertures. In early designs, circular apertures were extensively studied because the shape was easy to fabricate through wet-etch processes [2]. With the help of Focused Ion Beam (FIB), virtually any shape is obtainable. Still, to date there have not been many reports of comparisons of apertures in the near field with different geometries, even for some simple ones.

In this paper, we report studies of some of these simple aperture geometries fabricated on VSALs, including rectangular apertures with different aspect ratios as well as circular apertures. We have examined the effect of aperture geometry on the power throughput, while holding the aperture area constant to facilitate interpretation of the results. We use three methods, far-field power measurement, near-field measurement, and finite difference time domain (FDTD) simulation. The far-field measurement takes place at a distance $>> \lambda$ (the wavelength of the light source) from the aperture using far-field optics while the near-field measurement is performed at a distance $< \lambda/20$ from the aperture.

*Correspondent: Email: fchen@andrew.cmu.edu; Phone: 412-268-4989; Fax: 412-268-3245

Optical Data Storage 2003, Michael O'Neill, Naoyasu Miyagawa, Editors,
SPIE Vol. 5069 (2003) © 2003 SPIE · 0277-786X/03/$15.00

2. FABRICATION

The same procedures to fabricate VSALs from commercial laser diodes were used as reported previously [3]. Laser diodes of wavelength 655nm, and a nominal power of 10mW from the same batch were used. A Micrion 2500 focused ion beam etcher (FIB) with 10nm beam resolution was used to make the apertures. Three different apertures geometries were fabricated on the VSALs and the images are shown in Fig. 1. All apertures studied have the same area, 0.02 μm^2: two rectangular apertures have the same dimension of 100nm×200nm but oriented at 90 degrees with respect to each other, and one circular aperture with a radius of 80nm.

The apertures are below the ridge structure that confines the injected current. The active layer of the laser is in the X-direction underneath the apertures. The thickness of the active laser is typically from 0.2μm to 0.25μm (in the Y-direction). It is important to note that the emitted optical field from the laser is linearly polarized with polarization in the active layer direction (X-direction). Apertures are etched through a 50nm Al layer, which has the lowest skin depth (~16nm) among those metals used as reflectors at this wavelength.

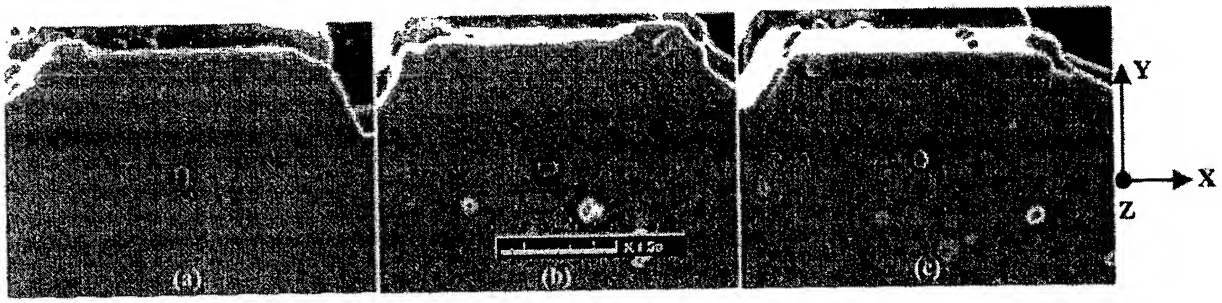

Figure 1: VSALs fabricated with apertures of different geometries: (a) 100nm×200nm; (b) 200nm×100nm; and (c) circular aperture with radius of 80nm. The E-field of the laser emission is in the horizontal (X) direction.

3. FAR-FIELD MEASUREMENTS

Previously, we used a far-field measurement technique to characterize the VSAL power throughput for rectangular nano-apertures [4]. It is interesting to point out that rectangles or squares have been a default aperture geometry on VSALs because circular apertures are not as simple to fabricate when using FIB. However, with the bitmap function of the FIB one can design more complicated structures and fabricate circular apertures rather nicely (Fig. 1).

We have previously shown the validity of treating nano-apertures as cutoff waveguides [4]. This approach provides a first-order approximation and explanation for the exponential decay of the optical field inside the aperture and also suggests that the orientation of the rectangular aperture plays an important role in the power throughput. It is intuitive to guess that the throughput of the circular aperture *c* would be intermediate between the two rectangular apertures *a* and *b*, as the orientation of the polarization of incident light does not matter for *c*, while there is always a favored orientation for the rectangular aperture.

The far-field measurement was performed using an objective lens of NA=0.65 and a high sensitivity power meter (Newport 1830c). The aperture emission power was separated from other noise emissions such as the back mirror emission in order to obtain clean aperture power. The results of far field power measurements for the three apertures are summarized in Table 1. We have shown both the absolute powers in μW and power ratios normalized to aperture *a*, which has the highest throughput. The data listed are averages of several repeated measurements for the same type of aperture. We also ensured that for each set of measurements, all apertures were fabricated together in order to reduce the uncertainty due to fabrication process variation from run to run. The far field measurement results for the rectangular apertures are consistent with our previous measurements in [4]. That is, when the alignment of a rectangular aperture is such that the short side is parallel to the primary incident polarization (along the active layer direction), the throughput is

higher. Furthermore, we found that the circular aperture value is intermediate between the two rectangular apertures as anticipated. Therefore, the circular aperture is not a better choice among other geometries.

Table 1. Aperture Power Throughput in Far-field

Aperture	a	b	c
Far-field Power (μW)	37.3	14	21
Throughput (Adjusted for N.A.)	100%	35%	58.6%

4. FDTD SIMULATIONS

We have simulated the optical fields in the vicinity of a nano-aperture when a linearly polarized elliptical Gaussian beam is incident on it. The free space wavelength of light chosen for the simulation was 650 nm. The thickness of the metal was 50nm. The numerical simulation was performed using the FDTD method [5]. In this method, the Maxwell's equations are discretized in space and time and are solved in the time domain using the Yee algorithm. The lossy nature of the aluminum metal was included by assuming a finite conductivity. Even though the simulation is carried out at a fixed optical frequency, the dispersion relation for the metal has to be included to prevent the simulation from becoming unstable during the transient initial phase of the simulation. A Lorentz dispersion relation for the metal [5] was chosen with the complex permitivity chosen to be a Lorentzian function of the frequency.

The incident beam was introduced in the X-Y plane using the total field/ reflected field formulation of the FDTD. The beam propagated in the positive Z direction. The resolution or the gird size chosen for the computational region was 4nm in all X, Y and Z directions. The simulation space in the X and Y directions is 400nm. Along the Z direction, we chose 40nm in the free space before the aperture and 120nm in the free space beyond the aperture.

We plotted the X-Y plane view of the Z-component of the Poynting vector for each aperture *a*, *b* and *c*, which are shown in Fig. 2 (a), (b) and (c) respectively. The Z plane was taken at the last grid point of the aperture on the exit side. From the gray scales over the apertures, we found that all have hot spots on the sidewalls in the X-direction, the incident field polarization direction. The time averaged Z-component of the Poynting vector was calculated and integrated over the X-Y plane. This is a measure of the far-field power transmitted (since the time averaged Z-component of the Poynting vector is zero for the evanescent, i.e. near-field components). The powers were normalized to that of aperture *a* and listed in Table 2. By comparison, aperture *a* has the largest output and *b* the smallest, while aperture *c* is in the middle. This is consistent with our far-field measurement results, with numerical differences due to the simulation being an ideal approximation.

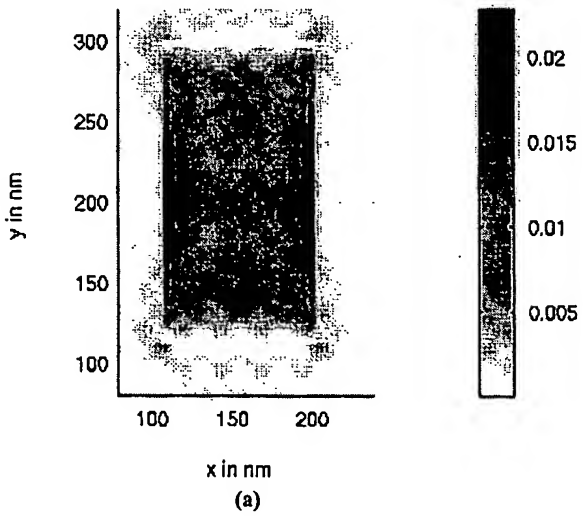

(a)

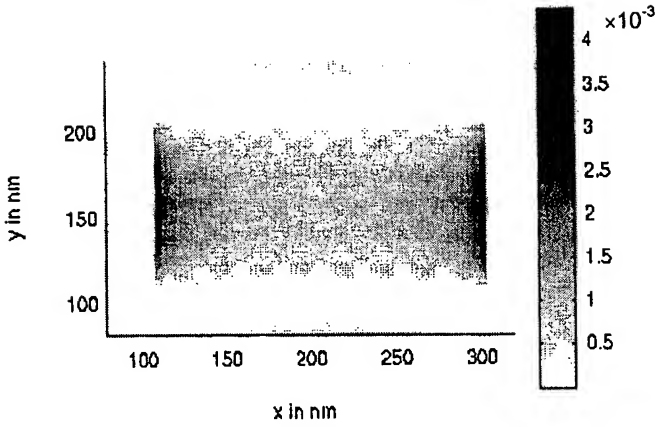

(b)

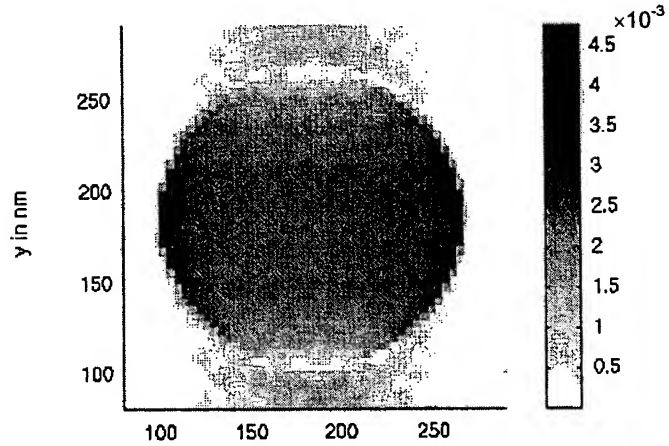

(c)

Figure 2: Time averaged Z-component of the Poynting vector of the transmitted field in the X-Y plane 2nm outside of the apertures: (a) 100nm×200nm, (b) 200nm×100nm, and (c) circular aperture with radius of 80nm.

Table 2. FDTD Simulation of the Relative Far-field Power Throughputs of the Three Different Apertures

Aperture	a	b	C
Relative Throughput to Aperture *a*	100%	10%	26%

5. NEAR-FIELD MEASUREMENTS

An intriguing question is, "Does a higher far field power necessarily imply a higher overall power throughput?" A near field measurement can compare the near-field signal strength of different apertures, and provides us with an answer to this question, and is complementary to the far-field measurements. Moreover, near-field measurements will provide light emission patterns and intensity distributions for the nano- apertures, and can be used to verify modeling results. The near-field measurement of the VSAL aperture light emission was carried out using an apertureless near-field scanning optical microscope (NSOM) [6]. The basic principle of the measurement is illustrated in Fig. 3. The VSAL is driven by a Melles-Griot laser driver to a lasing condition. The front facet is flat and the apertures are facing up. The light emitted from the aperture is scattered with a very sharp (30nm) AFM-like tungsten tip in close proximity to the aperture. The tip is driven to oscillate at a frequency *f*. The scattered light carrying the evanescent information of the optical field is transformed into a propagating field that can be collected by an objective lens and detected with an external photodiode. This signal is then demodulated with a lock-in amplifier where the signal at frequency *f* can be extracted. The software is then able to generate the images of the near-field signals simultaneously with the height images of the aperture.

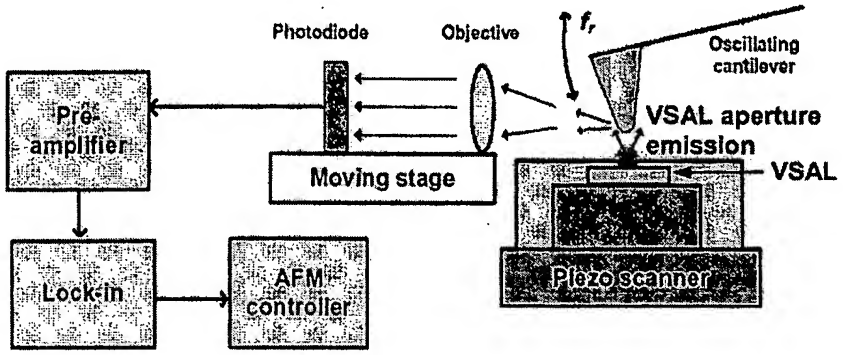

Figure 3: Apertureless Near-field Detection System Diagram

Utilizing this near-field measurement setup we were able to obtain aperture emission signals by demodulating at both *f* and *2f*, where *f* is the tip oscillation frequency [7]. For calibration purpose, the signal scattered by the tip was plotted against the tip-aperture separation as shown in Fig. 4. The two nearly overlap curves represent tracing and retracing processes of the tip motion relatively to the aperture in the Z-direction. It can be seen that the detected optical signal above the VSAL aperture decaying with increasing tip and aperture distance beyond 80nm, a signature property of near field signals. The drop of signal below 80nm is due to the decreased amplitude of tip oscillation as the tip approaches the surface.

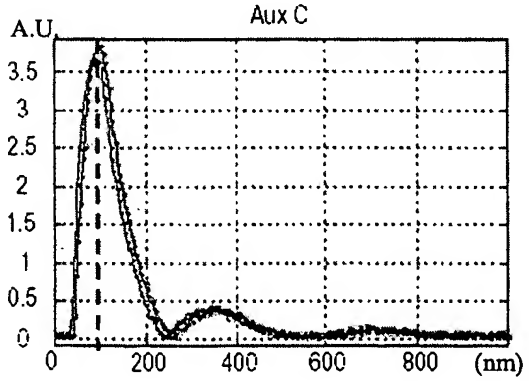

Figure 4: Detected aperture signals vs. tip and aperture distance

Multiple apertures can be fabricated on the same VSAL facet for near-field comparison. This makes VSALs an excellent nano-aperture testbed. This is demonstrated in Fig. 5 where apertures a, and b were fabricated to the right and left hand side of the centerline of the laser ridge structure. They are equally spaced from the centerline to ensure the fairness of the comparison. Once again, *a* is a rectangular aperture with its long side perpendicular to active layer and *b* is a rectangular aperture with long side parallel to active layer, where the active layer position is indicated with arrows.

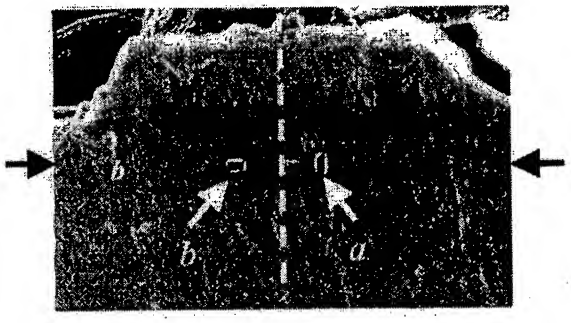

Figure 5: FIB image of multiple rectangular apertures fabricated on the same VSAL for near-field comparison

The near-field images of the aperture emissions detected at *1f* are shown in Fig. 6. Fig. 6 (a) shows that aperture *b* which is oriented with its long side parallel to the active region shows a much weaker signal than *a*, even though both are of equal distance from the center of the ridge. Fig. 6 (b) and (c) are the zoomed-in near-field emission pattern of each aperture. Notice that the aperture emission in Fig. 6 (b) does not look like a rectangle due to the fact that lower left corner of the aperture was blocked by a dust particle. Also note the hot spots on both sides of the aperture along the incident field direction in Fig. 6 (c). We found that the peak intensity ratio of *a:b* is 4.8× in the near-field. This can be compared to a measured far-field power ratio of 2.9× and a far-field power ratio of 10× in FDTD simulation. Thus we see that the aperture with a larger far-field power also shows more power throughput in the near-field.

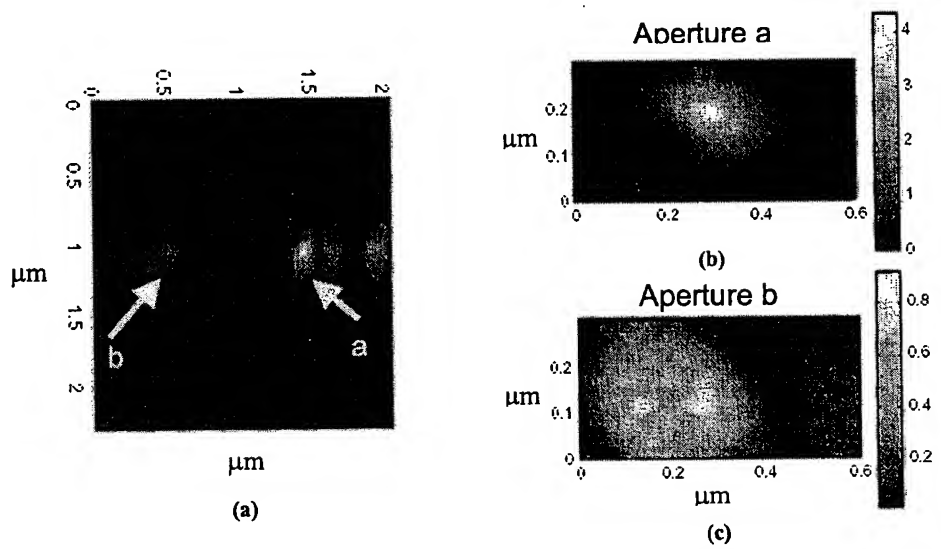

Figure 6: Near-field emission patterns of the aperture geometry effect of two 100nm×200nm apertures orientated 90° to each other: (a) large scan area shows that the one with the long side vertical to the active layer has a stronger output; (b) zoomed in on aperture *a*; (c) zoomed in on aperture *b* (notice the hot spots)

6. CONCLUSIONS

We have employed three different methods to characterize near-field nano-apertures fabricated on VSALs. We were able to quantitatively verify the aperture geometry dependent power throughput in far-field, near-field as well as in FDTD numerical modeling. From both far-field measurements and FDTD simulation results, we conclude that for apertures of the same area, a rectangular aperture with the long side perpendicular to the active layer has the largest throughput, while a circular aperture has the second largest, and the rectangular aperture with the long side parallel to the active layer has the least throughput among the three. The idea of using VSALs as a near-field aperture testbed was proposed and demonstrated. Multiple apertures may be fabricated on the same VSAL for comparison purposes. An apertureless NSOM was used for near-field nano-aperture imaging. We found that for the two rectangular apertures being studied, the near-field power throughput was consistent with the far-field power throughput. In conclusion, aperture geometry affects aperture total power throughput significantly and therefore designing high efficiency aperture structures is possible.

7. ACKNOWLEDGEMENT

This work was performed as part of the INSIC HAMR ATP Program, with the support of the U.S. Department of Commerce, National Institute of Standards and Technology, Advanced Technology Program, Cooperative Agreement Number 70NANB1H3056.

REFERENCES

1. A. Partovi, D. Peale, M. Wuttig, C. Murray, G. Zydzik, L. Hopkins, K. Baldwin, W. Hobson, J. Wynn, J. Lopata, L. Dhar, R. Chichester, and J. Yeh "High-power laser light source for near field optics and its application to high-density optical data storage," Appl. Phys. Lett. **75**, 1515 (1999).
2. P. Minh, T. Ono, and M. Esash, "Nonuniform silicon oxidation and application for the fabrication of aperture for near-field scanning optical microscopy," Appl. Phys. Lett. **75**, 4076 (1999).
3. F. Chen, J. Zhai, D. Stancil, and T. Schlesinger, "Fabrication of very small aperture laser (VSAL) from a commercial edge emitting laser," Jpn. J. Appl. Phys. **40**, Part 1, No. 3B, 1794 (2001).
4. F. Chen, D. Stancil, T. Schlesinger, "Aperture shape effect on the performance of very small aperture lasers (VSAL)," J. Appl. Phys., **93**, No. 10, 5871-5875 (2003).
5. A. Taflove, Computational Electrodynamics: The Finite Difference Time Domain Method, Artech House, (1995).
6. B. Akhremichev, S. Pollack, G. Walker, "Apertureless scanning near-field infrared microscopy of a rough polymeric surface," Langmuir, 17, 2774-2781 (2001).
7. B. Akhremitchev, Y. Sun, L. Stebounova, G. Walker, "Monolayer-sensitive infrared imaging of DNA stripes using apertureless near-field microscopy," Langmuir, 18, 5325-5328 (2002).